scientific reports

OPEN

Multiple ionization of iodine for 2.5–5.0 MeV I^{22+} ions impacting on Fe target

Xianming Zhou[1,3]✉, Jing Wei[1], Rui Cheng[2], Changhui Liang[1], Yanhong Chen[2], Xiaoan Zhang[1,2] & Yongtao Zhao[2,3]

The L-shell X-ray emissions of iodine are investigated as a function of the incident energy for I^{22+} ions impacting on Fe target in the energy region near the Bohr velocity. Six distinct L-subshell X-rays, Lι, L$\alpha_{1,2}$, L$\beta_{1,3,4}$, L$\beta_{2,15}$, Lγ_1 and L$\gamma_{2,3,4,4'}$, are observed. Compared to the atomic data, the energy of the experimental X ray shifts to the higher energy side. The relative intensity ratios of Lι, L$\beta_{1,3,4}$, L$\beta_{2,15}$, to L$\alpha_{1,2}$, Lι to L$\beta_{2,15}$ and L$\gamma_{2,3,4,4'}$ to Lγ_1 are enhanced, but has no obvious change with the increase of projectile energy in the present energy region. That is interpreted by the multiple ionization effect of the M-, N- and O-shell electrons.

The study of inner-shell ionization induced by highly charged ion-atom collisions can not only provide fundamental data for theoretical simulation of atomic-molecular reaction dynamics and analysis of cosmic astrophysics, but also have important practical applications in material modification, elemental analysis, warm and dense plasma diagnostics and so on[1–5]. Since the 1950s, due to the development of accelerator technology and the advancement of detection and analysis method, the related research has received extensive attention and made great achievements[6–48]. During the interaction of highly charged heavy ion with solids, above the target surface, the incident ions can capture the valance electrons of the surface target atoms to the high Rydberg state trough resonant capture to form the first hollow atoms (HA1)[22–24]. Then, it can enter the lower surface to interact with the target atoms at close range, and capture electrons from the inner-shell of the target atom to the shell with a smaller main quantum number in the way of side feeding, and form a more compact hollow atom (the second hollow atom, HA2) to achieve the neutralization[25,26]. In addition, the inner shell electrons of target atoms and projectile ions can be ionized by Coulomb collisions. The de-excitation of these excited atoms can emit X rays in the form of radiation, or excite Auger electrons in the form of radiationless Auger transition and CK (Coster-Kornig) transition[27,28]. The energy and broadening of characteristic X ray reflect the energy level structure and electron distribution of excited atoms. The X-ray production cross section can give the information of ionization probability of inner shell electrons[29–32]. So, X-ray emission measurement is an important method to experimentally study the atomic characteristics and the mechanism of atomic inner-shell ionization process in ion-atom collisions.

Previous studies on the interaction of highly charged ions with atoms can be divided into two categories. One is in the low energy region below the Bohr velocity. Experimentally, taking the research of Briand et al. as an example[33–36], using a crystal spectrometer, the formation mechanism of hollow atoms near the target surface was expounded through the high resolution structure analysis of K-shell X-ray. In theory, Burgdörfer established a classical over-the-barrier model (COBM) to describe this process[37]. The other is concentrated in the energy range of tens to hundreds MeV. Through the experimental measurement and theoretical analysis of X-ray emission cross section, the ionization of the inner shell is studied. And many well-established theories are developed to simulate such process, such as, Binary Encounter Approximation (BEA), Plane Wave Born Approximation (PWBA) and ECPSSR model (PWBA modified by Energy-loss, Coulomb-deflection, and Perturbed-Stationary-State Relativistic)[38–40]. However, in the energy region near the Bohr velocity, due to the limitation of experimental conditions, the relevant experimental research is relatively rare, and the theoretical description is still inconclusive.

Different from the neutralization de-excitation of the first and second generation hollow atoms formed by low velocity ions near the solid surfaces, the inner shell process generated by the impact of highly charged ions

[1]Ion Beam and Optical Physics Joint Laboratory of Xianyang Normal University and IMP, CAS, Xianyang Normal University, Wenlin Rd. 01, XianyangShannxi 712000, China. [2]Institute of Modern Physics, Chinese Academy of Sciences, Lanzhou 730000, China. [3]School of Science, Xi'an Jiaotong University, Xi'an 710049, China. ✉email: xmzhou19860208@163.com
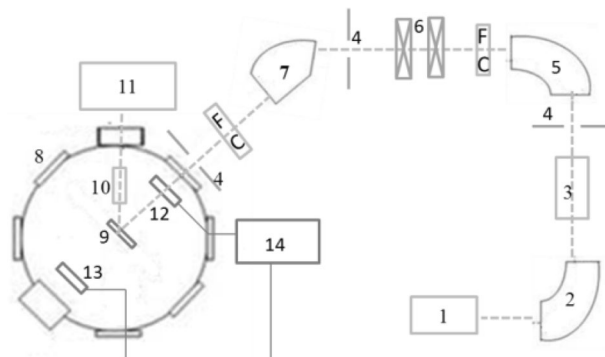
Figure 1. Schematic drawing of experiment setup: 1, ECR ion source, 2, analyzing magnet, 3, high volt accelerate platform, 4, barrier, 5, 90° deflection magnet, 6, magnetic quadrupled lens, 7, 60° deflection magnet, 8, ultrahigh vacuum target chamber, 9, target, 10, silicon drift detector, 11, X-ray recording system, 12, penetrable faraday cup, 13, common faraday cup, 14, projectile number recording system.

near the Bohr velocity has its own uniqueness. In addition to the neutralization process of electron capture, the projectile has enough energy to enter the target and interact with the target atoms in a close distance, and that result in Coulomb ionization. With the de-excitation of the holes in the inner shell, the outer shell may be in a multiple ionization state. That causes an energy shift of the X ray and a change in the relative intensity ratio of the sub-shell X ray. In our previous work, such multiple ionization of projectile has been observed and the effect of charge state and target atomic number has been verified[16,41]. Here, we would like to present the further research, and the special attention will be devoted to the influence of incident energy on the multiple ionization.

In this work, the highly charge heavy ions of I^{22+} with energy from 2.5 to 5.0 MeV (the velocity is about 0.89 to 1.26 times v_0, $v_0 = 2.19 \times 10^6$ m/s is the Bohr velocity) were used to bombard the solid Fe target. The L-subshell X rays were detected. The emission, energy shift and relative intensity ratio of the X rays were analyzed. The formation of multiple ionization states of the projectile and its effect on the X-ray emission were discussed.

Experimental method

The measurements have been carried out at the 320 kV high voltage experimental platform at the Institute of Modern Physics, Chinese Academy of Sciences (IMP, CAS) in Lanzhou, China. More details of the experimental system have been described in a previous work[42]. The experimental setup is shown in Fig. 1. In brief, the I^{22+} ions are produced and extracted from the Electron Cyclotron Resonance (ECR) ion source and selected by a 90° analyzing magnet, and then introduced into the ultrahigh vacuum target chamber (10^{-8} mbar) after acceleration, focus, multi-deflections and multi-collimations. The divergence of the beam is smaller than 0.2°. The ion beam impacts perpendicularly onto the target with a spot size of about Φ 3 mm. The target, prepared carefully in the laboratory, having a purity of 99.99% with surface area of 15×20 mm^2 and a thickness of 0.1 mm, is positioned on a sample holder. It permitted a three-dimensional movement to change freely the target position and remove away from the beam line in order to measure the current.

The emitted X-rays are detected by a Silicon Drift Detector (SDD) produced by AMPTEK. The SDD has an effective detection area of 7 mm^2 and a 12.5 μm Be window in the front of the detector. The SDD is placed at 80 mm far away from the target surface in the chamber and at 135° angle with respect to the beam direction. The detector has an effective energy range of 0.5–14.3 keV when the gain was selected at 100, and an energy resolution of about 136 eV at 5.9 keV. The energy calibration is performed using simultaneously two standard radioactive sources of ^{55}Fe and ^{241}Am, and then tested by measuring the energies of the K-shell X ray of Al, V and Fe produced by photon irradiation. In this way, a precise measurement of the X-ray energy can be guaranteed. The SDD intrinsic efficiency, which combines the effects of transmission through the Be window and the interaction in the silicon detector, is well determined by transmission measurement.

The number of incident projectiles, which could not be measured immediately by recording the target current due to the influence of the secondary electron emission, is detected indirectly by the combined use of a penetrable Faraday cup and a common one. Before every measurement, the projectile number detected by the penetrable Faraday cup (N_1) and the common Faraday cup (N_2) were recorded. The ration (R) of N_2/N_1 was checked. During the X-ray detection, the projectile number detected by the penetrable Faraday cup (N_1') was recorded. Therefore, the number of the projectile impacting on the target (N) could be calculated by the formula of $N = N_1' * R$.

Results and discussion

L-shell X-ray emission of iodine. In Fig. 2, the typical X-ray emission spectra of I for I^{22+} ions impacting on Fe target are presented as a function of incident energy. The spectra are normalized by the projectile number and well fitted by a nonlinear curve Gaussian fitting program. The structures of the spectra are similar for projectile with different energy. It consists mainly of six distinct L-subshell lines and can be identified as Lι, L$\alpha_{1,2}$, L$\beta_{1,3,4}$, L$\beta_{2,15}$, Lγ_1 and L$\gamma_{2,3,4,4'}$ X ray, which results from the radiation transition of M_1–L_3, $M_{5,4}$–L_3, M_4–L_2/$M_{3,2}$–L_1, $N_{5,4}$–L_3, N_4–L_2 and $N_{3,2}$–L_1/$O_{3,2}$–L_1, respectively[43,44].
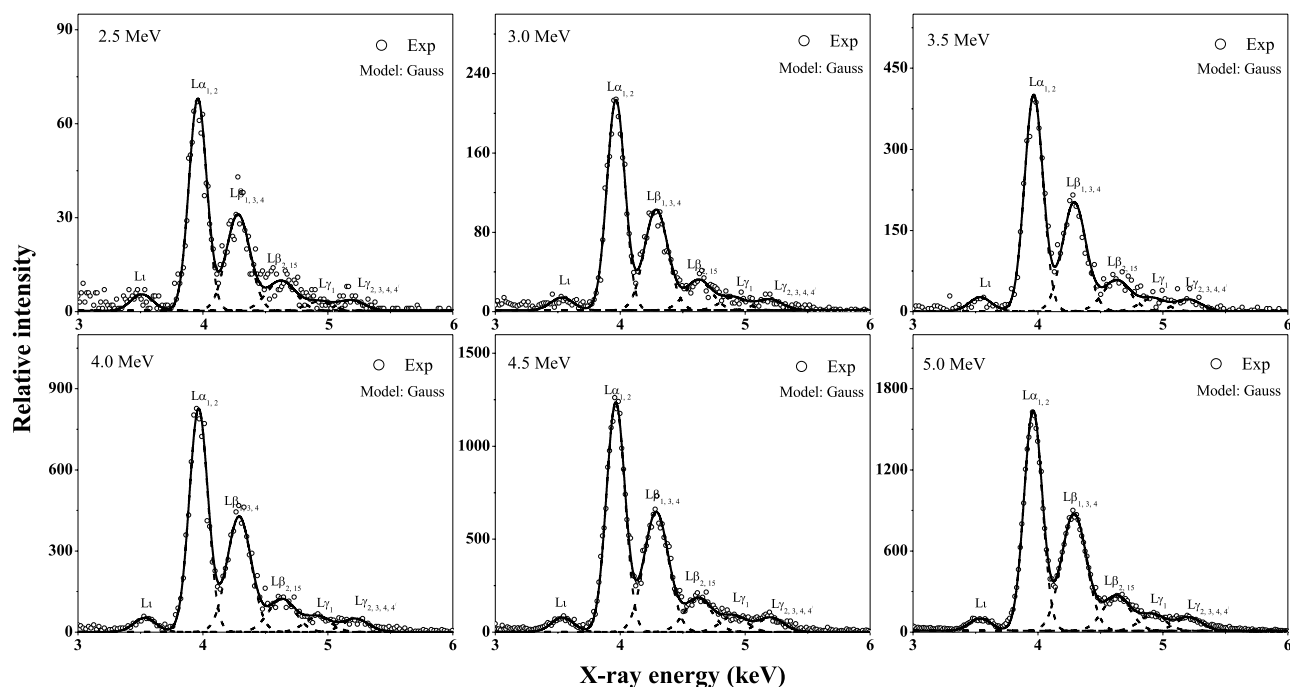
2

Figure 2. Characteristic X-ray spectra of I for I^{22+} ions with various incident energy impacting on Fe target.

Incident energy (MeV)	Lι (eV) ± 5 eV	Lα$_{1,2}$ (eV) ± 3 eV	Lβ$_{1,3,4}$ (eV) ± 5 Ev	Lβ$_{2,15}$ (eV) ± 5 eV	Lγ$_1$ (eV) ± 7 eV	Lγ$_{2,3,4,4'}$ (eV) ± 9 eV
2.5	3535	3960	4284	4625	4913	5190
3.0	3534	3959	4286	4622	4909	5192
3.5	3538	3965	4287	4626	4912	5195
4.0	3536	3966	4289	4625	4916	5207
4.5	3538	3965	4289	4627	4907	5201
5.0	3537	3964	4287	4623	4916	5208
Average	3536	3963	4287	4625	4912	5199
Atomic[43,44]	3485	3937	4227	4508	4802	5065
Shift	51	26	60	117	110	134

Table 1. The energies of I L-subshell X-rays produced by I^{22+} ions with various incident energies impacting on Fe target.

In the present work, the velocity of 2.5–5.0 MeV I^{22+} ions is about $(1.94–2.75) \times 10^6$ m/s. The distance between the ion source and the target surface is about 12.74 m. Taking into account the movement before acceleration, the minimum flight time of the incident ions to the target surface is also greater than 3.62×10^{-6} s. This is long enough for any decay of the projectile's original metastable. So, the present results can be eliminated for the decay of metastable state above the target surface. The initial electronic configuration of the projectile I^{22+} ion is [Ar] $3d^{10}4s^24p^1$. There is no initial L-shell vacancy. Therefore, the experimental spectrum is not the result of the de-excitation of the first generation hollow atoms on the upper surface. However, the corresponding holes and upper-level electrons are prerequisite for L-shell X-ray emission. The present experimental result indicates that, along with the neutralization process of electron capture, the inner-shell electrons of the incident ion are also ionized by collisions with the target atom within the target, and the second hollow atoms are formed. In the present work, the L-subshell X rays of I mainly come from the de-excitation of the second hollow atom below the surface.

Multiple ionization state of iodine ions. The measured energies of the six I L-subshell X ray are tabulated in Table 1. There are no obvious regular changes for different incident energy, and it is almost a constant within the estimated error, but larger than the value of a singly ionized atom[43,44]. For example, an average blue shift of 51±5 eV, 26±3 eV, 60±5 eV, 117±5 eV, 110±7 eV and 134±9 eV for Lι, Lα$_{1,2}$, Lβ$_{1,3,4}$, Lβ$_{2,15}$, Lγ$_1$ and Lγ$_{2,3,4,4'}$ X ray is observed, respectively. According to the discussion of section 'L-shell X-ray emission of iodine', the L X-ray emission of I occurs after the collisions below the surface, where the projectile has been slowed down due to the energy loss of collision, even though the initial velocity of I^{22+} ions is larger. Therefore, the effect of Dop-

pler shift on the line shift can be neglected. It is proposed that the observed blue shift arise primarily from the multiple ionization of outer-shell electrons, such as M-, N- and O-shell electrons.

During the collision of highly charged heavy ions with atoms, in addition to the ionization of inner-shell electrons, the multiple ionization state may be generated owing to the dual results of Coulomb ionization and electron capture. In this case, the screening of the nuclear is reduced because of the absence of outer-shell electrons, and the binding energies of the remaining orbital electrons are perturbed. As a result, the corresponding X-ray energy is enlarged, namely, the experimental blue shift is obtained. For example, the radiation energy of the M_5-L_3 transition for I atom is about 3939 eV, but that is about 3976 eV for I^{22+} ions, which is an increase of about 37 eV over the atomic data. So, it is proposed that, in the present work, in the interaction of the I^{22+} ions with the target atom, in addition to the single ionization of L-shell electrons, under the synergistic effect of ionization and capture, the M-, N- and O-shells form multiple ionization states which are different from the initial electron configuration.

If leaving the subsequent excitation by non-radiative transitions and the effect of electron correlation out of account, the multi-ionization cross section can be written in the form of the product of the single ionization cross section[45]. Multiple ionization degree is proportional to that of single ionization. Single ionization can be produced by Coulomb ionization or charger transfer. According to the estimation of PWBA theory and Oppenheimer–Brinkman–Kramer (OBK) approximation[46], the single ionization cross section of I L-shell produced by I^{22+} ions impacting on Fe target is in the order of 1 barn, and that is about 10^{5-6} barn for the M-shell electrons. The cross section increases with the increase of the incident energy, but the increase is not large, in the present experimental energy region. For example, the ionization cross section of $M_{4,5}$ electrons at the incident energy of 5 MeV is about 9 times larger than that at 2.5 MeV. This value is only about 3 and 6 for $M_{2,3}$ and M_1 electrons, respectively. Therefore, there should be no obvious change in the multi-ionization degree of the outer-shells with the incident energy. This can also be verified from the change in the relative intensity ratio of the sub-shell X rays, as discussed below. As a result, no obvious change in the blue shift of the experimental spectra line was observed with the incident energy, as shown in Table 1.

Influence of multiple ionization on the relative intensity ratios of the L-subshell X rays.

The multiple ionization not only causes the blue shift of the X-ray energy, but also affects the fluorescence yield of each subshell X rays. This will result in a change in the relative intensity ratio of the observed spectral lines. Figures 3, 4, 5, 6 and 7 show the relative intensity ratios of the L-subshell X ray as a function of the incident energy. The experimental error mainly comes from the X-ray count statistics, and the maximum value is about 10%. For comparison, the theoretical atomic data for single ionization are also given, which is obtained from the ECPSSR calculation. It can be found that the experimental values are larger than the theoretical atomic data and almost identical at different incident energy within the error. This can be understood in terms of the multiple ionization states of the projectile.

$L\beta_{1,3,4}$ X ray mainly contains three lines of the radiation transition from M electrons filling the L_2- and L_1-subshell vacancies. For iodine, the theatrical relative intensity ratio of M_4-L_2 (corresponding to $L\beta_1$ X ray) to $M_{3,2}$-L_1 (corresponding to $L\beta_{3,4}$ X ray) radiation transition is about 10 to 1[47,48]. $L\beta_{1,3,4}$ and $L\alpha_{1,2}$ X ray can be roughly regard as the main results of transitions of $M_{4,5}$ electrons to L_3 and L_2 vacancies, and the corresponding fluorescence yield is 0.021 and 0.038, respectively. The Auger yield a_2 and a_3 for the L_2 and L_3 subshell are 0.767 and 0.921[47,48]. They are all in the same order of magnitude, and not much different[47,48]. When the outer shells are in the multiple ionization states, the Auger transition probability of L_2 and L_3 vacancies will be reduced in the same proportion, and which will result in an enhancement of the fluorescence yield of the M_4-L_2 and $M_{5,4}$-L_3 transition by almost the same magnitude. So, this will not cause a significant change in the relative intensity ratio of $L\beta_{1,3,4}$ and $L\alpha_{1,2}$ X rays.

However, compared with the de-excitation of L_3 vacancies, that of L_2 has an additional effective channel, L_2–L_3X CK transition, besides the X-ray emission and Auger transition. Due to the absence of M-, N- and O-shell electrons in the multiple ionization, part of the CK transitions are suppressed, and the $L\beta_1$ X-ray emission will be enhanced correspondingly. In addition, there are three channels for the de-excitation of L_1 vacancies, which are X-ray emission, Auger transition and CK transition. The multiple ionization of M-. N- and O-shell will weakens the process of non-radiation transition, and lead to the enhancement of $L\beta_{3,4}$ X-ray emissions. As a whole result, the relative intensity ratios of $L\beta_{1,3,4}$ to $L\alpha_{1,2}$ X rays are enlarged, as shown in Fig. 3. This ratio is essentially constant with the incident energy. This further explains that the multiple ionization degree of outer shells is basically invariant with the projectile energy in the present work.

$L\beta_{2,15}$ and $L_{\alpha1,2}$ X rays mainly come from the transition of N and M electrons to the same lower energy level L_3, respectively. There are mainly two channels for the de-excitation of L_3 vacancies, Auger transition and X-ray emission. The sum of fluorescence yield ω_3 and Auger yield a_3 is unity: $\omega_3 + a_3 = 1$. When multiple electrons are absent in the shells such as M and N, the Auger transition filling the L_3 vacancies is decreased, and correspondingly, the X-ray emission is enhanced. For iodine, a_3 is about 2–3 orders of magnitude larger than ω_3 of L_3-subshell X rays. The probability of $M_{5,4}$–L_3 radiation transition is about 6 times as large as that of $N_{5,4}$–L_3 transition[47,48]. Therefore, the fluorescence yield of $L\beta_{2,15}$ X ray is more susceptible to multiple ionization. This will cause the relative intensity ratio of $L\beta_{2,15}$ to $L\alpha_{1,2}$ X ray to be greater than the atomic data. The extent of multiple ionization is almost independent of the incident energy. So, the ratio is almost constant with the increasing incident energy, as shown in Fig. 4.

In the same way, the ratio of $I(L\iota)/I(L\alpha_{1,2})$ can be understood easily. The fluorescence yield of $L\iota$ X ray is about 1/30 of that of $L\alpha_{1,2}$ X ray[47,48]. Therefore, the enhancement of $L\iota$ X-ray emission produced by the multiple ionization of M-, N- and O-shell is greater than that of $L\alpha_{1,2}$ X ray. As shown in Fig. 5, the relative intensity ratios of
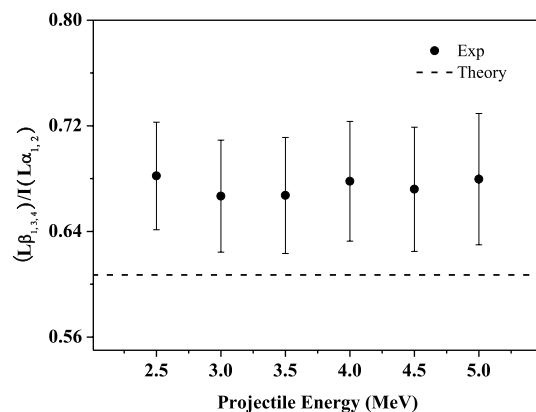
Figure 3. Relative intensity ratios of I L$\beta_{1,3,4}$ to L$\alpha_{1,2}$ X-ray as a function of incident energy.
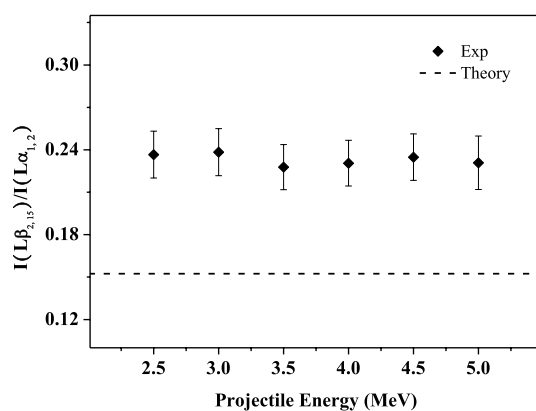

Figure 4. Relative intensity ratios of I L$\beta_{2,15}$ to L$\alpha_{1,2}$ X-ray as a function of incident energy.
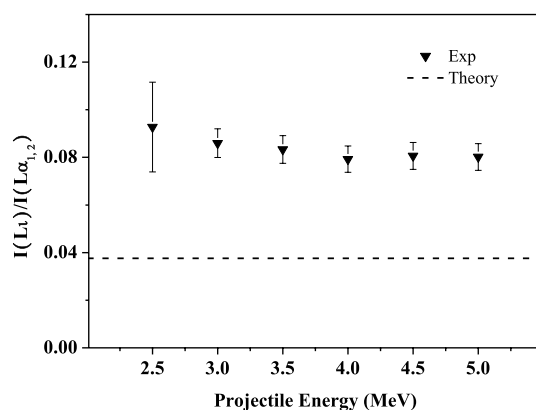

Figure 5. Relative intensity ratios of I Lι to L$\alpha_{1,2}$ X-ray as a function of incident energy.

Lι to L$\alpha_{1,2}$ X ray are higher than the theoretical data for single ionization atom, and have no significant change with incident energy duo to the independent of multiple ionization on projectile energy in the present work.

Theoretically, the fluorescence yield of the single ionized atomic $N_{4,5}$–L_3 transition is about 5 times larger than that of the M_1–L_3 transition. Compared to atomic data, the experimental enhancement of Lι X-ray emission will be larger than that of L$\beta_{2,15}$ X ray. As shown in Fig. 6, the experimental ratio of I(Lι)/I(L$\beta_{2,15}$) is about 1.5 times higher than the theoretical simulation. This also can be deduced from the results in Figs. 5 and 6, where it can be found that the experimental ratio of I(L$\beta_{2,15}$)/I(L$\alpha_{1,2}$) is about 1.5 times of the theoretical value, and that is about 2.2 for the ratio of I(Lι)/I(L$\alpha_{1,2}$). This is further verified that, the smaller the probability of radiation
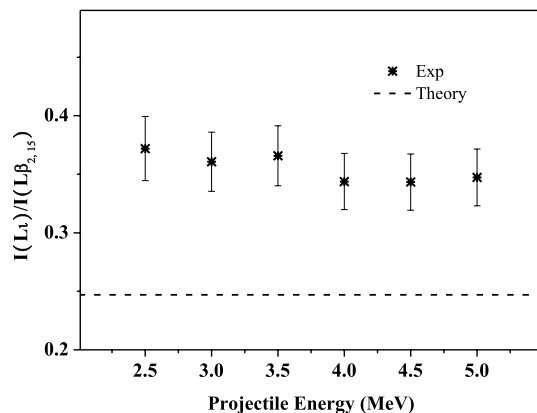
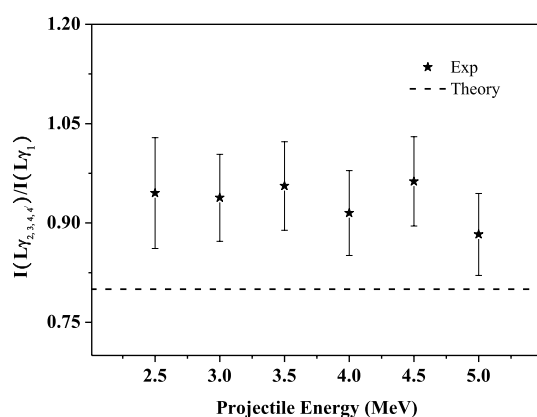**Figure 6.** Relative intensity ratios of I Lι to Lβ$_{2,15}$ X-ray as a function of incident energy.

Figure 7. Relative intensity ratios of I Lγ$_{2,3,4,4'}$ to Lγ$_1$ X-ray as a function of incident energy.

transition, the greater the change in fluorescence yield affected by the multiple ionization of the out shell, and the greater the enhancement magnitude of the corresponding X-ray emission.

Figure 7 presents the relative intensity ratio of Lγ$_{2,3,4,4'}$ to Lγ$_1$ X ray. It is clear that the measured value is larger than the theoretical data of single ionized atom, and the ratios are almost identical with increasing incident energy. This can be interpreted by analogy with the results in Fig. 3. Lγ$_1$ X ray comes from the radiation transition of N$_4$-L$_2$. Lγ$_{2,3,4,4'}$ X ray mainly consists of four lines for the radiation transitions of N$_3$/N$_2$/O$_3$/O$_2$-L$_1$. The fluorescence yield of those two X rays is 0.0028 and 0.0004, and the Auger yield a$_2$ and a$_1$ at the corresponding lower energy levels L$_2$ and L$_1$are 0.767 and 0.495, respectively[47,48]. The probability of Auger transition is about 2 to 3 orders of magnitude higher than that of radiation transition. This will result in a significant enhancement of the X-ray emission, under the influence of multiple ionization. The fluorescence yield of Lγ$_{2,3,4,4'}$ X ray is about one order of magnitude smaller than that of Lγ$_1$ X ray. Therefore, Lγ$_{2,3,4,4'}$ X-ray emission is more susceptible to multiple ionization. As a result, the ratio of I(Lγ$_{2,3,4,4'}$)/I(Lγ$_1$) will be enlarged. In addition, there has one more channel of L$_1$-L$_2$Y CK transition for the filling of L$_1$ vacancies than that of L$_2$ subshell. This will also lead to an increase in the fluorescence yield ω$_1$ for the de-excitation of L$_1$ vacancies. Taking the above two points into consideration, when the outer shells are multiply ionized. The fluorescence yield of Lγ$_{2,3,4,4'}$ X ray has a greater increase than that of Lγ$_1$. As a result, the experimental ratio of I(Lγ$_{2,3,4,4'}$)/I(Lγ$_1$) is larger than the theoretical value.

In summary, compared to the theoretical calculation, the experimental relative intensity ratio of the L-subshell X ray is enlarged and goes over 1.2–2.2 times the theory prediction, as shown in Figures 3, 4, 5 and 7. This provides another evidence for the multiple ionization state of the projectile. In the present experimental energy region, the multiple ionization degree is basically constant as the incident energy increases. With the multiple ionization in the M-, N- and O- shells, the fluorescence yield of L-shell X ray is enlarged, because the radiationless transition process is suppressed duo to the absence of some M-, N- and O-shell electrons. The smaller the fluorescence yield of the single ionized atom, the greater the change in the multiple ionization fluorescence yield. As a result, the observed relative intensity ratios are larger than the theory values. Each ratio is different owing to the various changes in fluorescence yield, but it is basically invariant with the change of incident energy.

Conclusions

I L-shell X-ray emission for 2.5–5.0 MeV I^{22+} ions impacting on Fe target was measured. The energy and the relative intensity ratio of the subshell X rays have been investigated as function of the incident energy. The results indicate that, in the energy region near the Bohr velocity, the projectiles undergo simultaneously the dual effects of ionization and electron capture during the interaction with target atoms below the surface. In addition to the neutralization, the I^{22+} ions are also ionized. Not only the L-shells are ionized, but also the outer-shells, such as M-, N- and O- shells, are multiply ionized. At the balance of ionization and electron capture, the M-, N- and O- shells remain multiple ionization states when the L-shell X-ray is emitted. This leads to a blue shift of the X-ray energy and an increase in the fluorescence yield. Moreover, the smaller the atomic fluorescence yield, the larger the increase in fluorescence yield caused by multiple ionization.

References

1. Prieto, J. E., Zucchiatti, A., Galan, P. & Prieto, P. Cross sections of X-ray production induced by C and Si ions with energies up to 1 MeV/u on Ti, Fe, Zn, Nb, Ru and Ta. *Nucl. Instr. Methods B* **406**, 167–172 (2017).
2. Mukoyama, T. *et al.* M-shell ionization cross sections by proton impaction gold in the binary-encounter approximation. *Nucl. Instr. Methods B* **354**, 155–158 (2015).
3. Wilhelm, R. A. *et al.* Interatomic coulombic decay: The mechanism for rapid deexcitation of hollow atoms. *Phys. Rev. Lett.* **119**, 103401 (2017).
4. Szabo, G. L. *et al.* Nano-hillock formation on CaF2 due to individual slow Au-cluster impacts. *Nanotechnology* **32**, 355701 (2021).
5. Ciricosta, O. *et al.* Direct measurements of the ionization potential depression in a dense plasma. *Phys. Rev. Lett.* **109**, 065002 (2012).
6. Orita, S. M. & Amiya, M. K. Inner-shell ionization by heavy charged particles. *Chin. J. Phys.* **5**, 199–228 (1977).
7. Arnau, A. *et al.* Interaction of slow multicharged ions with solid surfaces. *Surf. Sci. Rep.* **27**, 113–239 (1997).
8. Schenkel, T., Hamza, A. V., Barnes, A. V. & Schneider, D. H. Interaction of slow, very highly charged ions with surfaces. *Surf. Sci. Rep.* **61**, 23–84 (1999).
9. Baragiola, R. A. Invited review: Some challenging unsolved problems in atomic collisions in solids. *Nucl. Instr. Methods B* **237**, 520–524 (2005).
10. Miranda, J., deLucio, O. G. & Lugo-Licona, M. F. X-ray production induced by heavy ion impact: Challenges and possible uses. *Rev. Mex. Fís.* **53**, 29–32 (2007).
11. Aumayr, F., Facsko, S., El-Said, A. S., Trautmann, C. & Schleberger, M. Single ion induced surface nanostructures: A comparison between slow highly charged and swift heavy ions. *J. Phys. Condens. Matter* **23**, 393001 (2011).
12. Lapicki, G. The status of theoretical L-shell x-ray production cross sections by protons based on their revised universal empirical fit. *Nucl. Instr. Methods B* **467**, 123–129 (2019).
13. Shehla, *et al.* Measurements of the line resolved M-shell X-ray production cross sections for 79Au, 82Pb and 83Bi by 100 keV/u proton, C, N, O ions. *Nucl. Instr. Methods B* **399**, 74–82 (2017).
14. Schuch, R., Madzunkov, S., Lindroth, E. & Fry, D. Unexpected X-ray emission due to formation of bound doubly excited states. *Phys. Rev. Lett.* **85**, 5559–5562 (2000).
15. Czarnota, M. *et al.* X-ray study of M-shell ionization of heavy atoms by 8.0–35.2 MeV Oq+ ions : The role of the multiple ionization effects. *Phys. Rev. A* **79**, 032710 (2009).
16. Zhou, X. *et al.* I L-shell X-rays from near Bohr-velocity I20+ ions impacting on various targets. *Acta. Phys. Sin.* **70**, 023201 (2021).
17. Wei, J. *et al.* Mg K-shell x-ray emission induced by various ions. *Nucl. Instr. Methods B* **496**, 78–83 (2021).
18. Zhao, Y. *et al.* Benchmark experiment to prove the role of projectile excited states upon the ion stopping in plasmas. *Phys. Rev. Lett.* **126**, 115001 (2021).
19. Zhou, X. *et al.* X-ray emission for Ar11+ ions impacting on various targets in the collisions near the Bohr velocity. *Chin. Phys. B* **30**, 8083201 (2021).
20. Ren, J. *et al.* Charge-state dependence of inner-shell processes in collisions between highly charged Xe ions and solids at intermediate energies. *Phys. Rev. A* **92**, 062710 (2015).
21. Zhou, X. *et al.* Charge state effect on the K-shell ionization of iron by xenon ions near the Bohr velocity. *Chin. Phys. B* **22**, 113402 (2013).
22. Winecki, S., Cocke, C. L., Fry, D. & Stöckli, M. P. Neutralization and equilibration of highly charged argon ions at grazing incidence on a graphite surface. *Phys. Rev. A* **53**, 4228–4237 (1996).
23. Yamazaki, Y. A microcapillary target as a metastable hollow ion source. *Nucl. Instr. Methods B* **193**, 516–522 (2002).
24. Watanabe, H. *et al.* X-ray emission in collisions of highly charged I, Pr, Ho, and Bi ions with a W surface. *Phys. Rev. A* **75**, 062901 (2007).
25. Schenkel, T. *et al.* Ablation of GaAs by intense, ultrafast electronic excitation from highly charged ions. *Phys. Rev. Lett.* **81**, 2590–2593 (1998).
26. Briand, J. P. *et al.* Decay of hollow atoms above and below a surface. *Phys. Rev. A* **54**, 4136–4139 (1996).
27. Frederick, R. & Hirsh, J. Auger transitions. *Phys. Rev.* **69**, 32 (1946).
28. Sharma, M., Singh, P., Puri, S., Mehta, D. & Singh, N. L1–L3 Coster-Kronig yield for elements with 70⩽Z⩽81. *Phys. Rev. A* **69**, 032501 (2004).
29. Kobal, M. Ka and Kb satellite and hypersatellite fluorescence yields of Mg and Si. *Nucl. Instr. Methods B* **229**, 165–179 (2005).
30. Słabkowska, K. & Polasik, M. Effect of L- and M-shell ionization on the shapes and parameters of the K X-ray spectra of sulphur. *Nucl. Instr. Methods B* **205**, 123–127 (2003).
31. Jacobs, V. L., Davis, J., Rozsnyai, B. F. & Cooper, J. W. Multiple ionization and x-ray emission accompanying the cascade decay of inner-shell vacancies in Fe. *Phys. Rev. A* **21**, 1917–1926 (1980).
32. Awaya, Y., Kambara, T. & Kanai, Y. Multiple K- and L-shell ionizations of target atoms by collisionswith high-energy heavy ions. *Int. J. Mass Spctrom.* **192**, 49–63 (1999).
33. Briand, J. P. *et al.* Production of hollow atoms by the excitation of highly charged ions in interaction with metallic surface. *Phys. Rev. Lett.* **65**, 159–162 (1990).
34. Briand, J. P. *et al.* Subfemtosecond study of the hypersatellite-satellite cascade in "hollow" atoms. *Phys. Rev. A* **43**, 565–567 (1991).
35. d'Etat, B. *et al.* Interaction of Ar17+ ions on metallic surfaces at grazing incidence. *Phys. Rev. A* **48**, 1098–1106 (1993).
36. Briand, J. P. *et al.* Observation of hollow atoms or ions above insulator and metal surfaces. *Phys. Rev. Lett.* **77**, 1452–1455 (1996).
37. Burgdörfer, J., Lerner, P. & Meyer, F. W. Above-surface neutralization of highly charged ions: The classical over-the-barrier model. *Phys. Rev. A* **44**, 5674–5685 (1991).
38. Gryzinski, M. Classical theory of atomic collisions. I. Theory of inelastic collisions. *Phys. Rev.* **138**(2A), 336–358 (1965).

39. Johnson, D. E., Basbas, G. & McDaniel, F. D. Nonrelativistic plane-wave Born-approximation calculations of direct Coulomb M-subshell ionization by charged particles. *At. Data Nucl. Data Tables* **241**, 1–11 (1979).
40. Brandt, W. & Lapicki, G. Energy-loss effect in inner-shell Coulomb ionization by heavy charged particles. *Phys. Rev. A* **23**, 1717–1729 (1981).
41. Zhou, X. *et al.* L-subshell X-ray intensity ratio of Xenon for 6 MeV Xe^{20+} impact on selected targets. *Nucl. Instr. Methods B* **304**, 32–35 (2013).
42. Zhou, X. *et al.* K and L-shell X-ray production cross section for 50–250 keV proton impact on elements with Z = 26–30. *Nucl. Instr. Methods B* **299**, 32–35 (2013).
43. Bearden, J. A. X-ray wavelengths. *Rev. Mod. Phys.* **39**, 78–124 (1967).
44. *X-Ray Data Book*: http://xdb.lbl.gov/. *Table of Isotopes*: http://ie.lbl.gov/atom.htm.
45. Kavčič, M., Šmit, Ž & Budnar, M. L-shell ionization in near-central collisions of MeV protons with low-Z atoms. *Phys. Rev. A* **56**, 4675–4682 (1997).
46. Dewangana, D. P. & Eichle, J. Charge exchange in energetic ion-atom collisions. *Phys. Rep.* **247**, 59–219 (1994).
47. Krause, M. O. Atomic radiative and radiationless yields for K and L shells. *J. Phys. Chem. Ref. Data.* **8**, 307–327 (1979).
48. Crawford, J., Cohen, D., Doherty, G. & Atanacio, A. *Calculated K, L and M-shell X-ray Line Intensities for Light ion Impact on Selected Targets from Z= 6 to 100* (Australian Nuclear Science and Technology Organization, 2011).

Acknowledgements

Author contributions

X.Z. and Y.Z. conceived the idea and designed the experiment. X.Z., J.W., R.C., C.L., Y.C. and X.Z. carried out the experiment. X.Z. analyzed the data and wrote the manuscript. X.M. and J.W. reviewed the manuscript. Advices have been given by all the authors.

Competing interests

The authors declare no competing interests.

Additional information

Correspondence and requests for materials should be addressed to X.Z.

Reprints and permissions information is available at www.nature.com/reprints.

Publisher's note Springer Nature remains neutral with regard to jurisdictional claims in published maps and institutional affiliations.